https://doi.org/10.5194/egusphere-2025-2132
Preprint. Discussion started: 17 July 2025

Decoding multicomponent hydrochemical anomalies: A synergy anomaly detection model for earthquake forecasting in active tectonic zone

Weiye Shao[1], Ying Li[2,*], Xiaocheng Zhou[2,*], Zhi Chen[2], Huajiao Liu[3], Zhaofei Liu[2], Chang Lu[2], Yuwen Wang[2,4], Zhaojun Zeng[2,4], Yun Wang[5], Hongyi He[6,2], Shaohui Fan[1]

[1]Yunnan Earthquake Agency, Kunming 650224, China

[2]United Laboratory of High-Pressure Physics and Earthquake Science, Institute of Earthquake Forecasting, Beijing 100036, China

[3]Sichuan Earthquake Agency, Chengdu 610041, China

[4]School of the Earth Sciences and Resources, China University of Geosciences, Beijing 100083, China

[5]Department of Insurance, School of Finance, Yunnan University of Finance and Economics, Kunming 650221, China

[6]Key Laboratory of Shale Gas Exploration, Ministry of Natural Resources, China University of Petroleum, Beijing 102249, China

Correspondence to: Ying Li (liying@ief.ac.cn), Xiaocheng Zhou (zhouxiaocheng188@163.com).

https://doi.org/10.5194/egusphere-2025-2132
Preprint. Discussion started: 17 July 2025

Abstract

The intersection of the Xiaojiang Fault and the Red River Fault at the southeastern margin of the Tibetan Plateau experiences intense tectonic activity. At this intersection, frequent destructive earthquakes have induced hydrochemical variations in thermal springs. In this study, Bayesian change point analysis is applied, and a multicomponent synergy anomaly detection model is developed using five years of monitoring data (2019–2024) from two thermal springs in the region to achieve real-time forecasting of occurrence timing for $M \geq 4$ earthquakes. Comprehensive analysis demonstrates that the anomaly detection model possesses reliable real-time anomaly detection capabilities. Tailored model parameters for specific hydrochemical components account for their differences in response characteristics to seismic activity. The model identifies Na^+, Ca^{2+}, Cl^-, SO_4^{2-}, δD, and $\delta^{18}O$ as sensitive indicators for strong earthquake forecasting. The multicomponent synergy alarm mechanism for hydrochemistry overcomes the limitations of single-parameter methods, which significantly enhances the model's overall performance in earthquake forecasting. The number of hydrochemical components with synchronous anomalies serves as a reliable criterion for determining alarm intensity, with higher intensity typically correlating with larger earthquake magnitudes or shorter epicentral distances.

Keywords:

Thermal springs, Hydrogeochemistry, Multicomponent synergy, Anomaly detection model, Earthquake forecasting

https://doi.org/10.5194/egusphere-2025-2132
Preprint. Discussion started: 17 July 2025

1. Introduction

Earthquake forecasting, a frontier in geosciences, relies on detecting sensitive and reliable precursor anomalies (Chen, 2009; Pritchard et al., 2020). Subsurface fluids, owing to their ease of migration and incompressibility, respond rapidly to dynamic crustal stress changes during earthquake preparation. These responses often result in significant changes in the physicochemical properties of the fluids (Lee et al., 2017; Gori & Barberio, 2022; Tian et al., 2023). Moreover, subsurface fluids can transmit deep geological signals to the surface, for example, through thermal springs, which makes them valuable targets for monitoring precursor anomalies. Currently, earthquake-related anomalies in subsurface fluids are widely monitored across various spatial and temporal scales. These include hydrological anomalies such as water temperature, water level, and flow rate (Shi et al., 2015; Lee et al., 2017; Petitta et al., 2018; Di Matteo et al., 2020; Du et al., 2023), hydrogeochemical anomalies like major elements, trace elements, and stable isotopes (Ide et al., 2020; Nakagawa et al., 2020; Barbieri et al., 2021; Wang et al., 2021; Zhang et al., 2021; Yan et al., 2022), and gas geochemical anomalies such as radon, helium, and carbon dioxide (Chaudhuri et al., 2011; Fu et al., 2017; Woith et al., 2020; Zhao et al., 2021; Zhou et al., 2021). While some fluid precursor anomalies have shown predictive value, many are still identified only through retrospective analysis after earthquakes. Moreover, continuous fluid monitoring data often reflect integrated signals from multiple sources, including seismic activity, environmental variability, and human-induced influences (Martinelli, 2020). The isolation of true seismic precursor anomalies from such complex datasets remains a significant challenge in current earthquake forecasting research.

In analysing large-scale fluid monitoring data, traditional anomaly detection methods typically

https://doi.org/10.5194/egusphere-2025-2132
Preprint. Discussion started: 17 July 2025

rely on manually defined fixed thresholds to identify fluctuations. Techniques such as trend analysis and standard deviation methods offer clear advantages in capturing prominent anomalies (Ingebritsen & Manga, 2014; Yan et al., 2018). However, in practice, fluid monitoring data often integrate superimposed signals from both tectonic and non-tectonic sources and exhibit complex nonlinear dynamic behaviors. These characteristics present notable limitations for traditional statistical approaches in effectively identifying fluid precursor anomalies (Yan et al., 2021). Machine learning-based anomaly detection algorithms offer new perspectives for earthquake forecasting by uncovering hidden precursor signals within large volumes of monitoring data (Li et al., 2022, 2023). In recent years, algorithms such as artificial neural networks, long short-term memory networks, and random forests have been widely applied to anomaly detection in individual indicators, such as water levels and radon concentrations, significantly enhancing detection accuracy and sensitivity (Tareen et al., 2019; Haider et al., 2021; Feng et al., 2022; Zhang et al., 2025). However, single-indicator measurements are easily influenced by meteorological, tidal, and other environmental factors. While regression models and similar techniques have been used to correct these interferences, challenges remain in effectively distinguishing non-seismic anomalies (Woith, 2015; Soldati et al., 2020). Moreover, single-indicator analysis does not leverage the synergistic relationships among multiple indicators, which thus limits its ability to enhance the reliability of anomaly identification.

Thermal springs are natural discharge outlets of deep-circulating groundwater and they offer distinct advantages for hydrogeochemical monitoring. The hydrochemical components (e.g., Na^+, Cl^-, SO_4^{2-}) of thermal springs tend to exhibit high stability, rapid upward migration, and limited susceptibility to environmental interference. These characteristics help minimise non-seismic noise

https://doi.org/10.5194/egusphere-2025-2132
Preprint. Discussion started: 17 July 2025

and allow for a more accurate reflection of hydrogeological changes during earthquake preparation (Martinelli, 2020; Tian et al., 2024). Numerous studies have reported diverse geochemical behaviors among hydrochemical components, which shows marked differences in their response magnitude, quantity, patterns, and timing to tectonic stress variations throughout the earthquake preparation process (Li et al., 2021; Yan et al., 2022; Tian et al., 2023). Therefore, applying anomaly detection algorithms to evaluate the abnormal response characteristics of individual hydrochemical components and integrating multiple components to enhance anomaly identification accuracy may represent a promising technical approach for precursor recognition. Current research on hydrochemical anomaly detection algorithms remains in an exploratory stage (Castellana & Biagi, 2008). Existing studies have demonstrated the effectiveness of common machine learning algorithms in identifying abnormal periods in hydrochemical data while also emphasising the need for scenario-specific optimisation of key indicators (Zhu et al., 2024). However, there is an urgent need to investigate the synergistic anomaly response patterns among hydrochemical components and to identify sensitive indicators for reliable forecasting of strong earthquakes.

This study focuses on the tectonically active region at the intersection of the Xiaojiang Fault (XJF) and the Red River Fault (RRF) on the southeastern margin of the Tibetan Plateau. The real-time anomaly was innovatively modified using the detection algorithm developed by Piersanti et al. (2016), and its application was extended to the analysis of multiple hydrochemical components in thermal springs across the study area. By integrating continuous monitoring data of hydrochemical ions and hydrogen–oxygen isotopes with earthquake catalogs and applying Bayesian change point (BCP) analysis, this study optimised parameters for specific components and built a multi-component joint

https://doi.org/10.5194/egusphere-2025-2132
Preprint. Discussion started: 17 July 2025

anomaly detection model. This model supports anomaly detection in both long-term time series and real-time earthquake forecasting across different time scales. The main objectives of this study are as follows: (1) to evaluate the applicability and performance of the algorithm in analysing hydrochemical time series; (2) to identify effective hydrochemical indicators for forecasting strong earthquakes in the study area; and (3) to assess the feasibility of the multi-component joint anomaly detection model and explore the relationship between hydrochemical variations and seismic activity by analysing the number of components with synchronous anomalies.

2. Geological setting

The southeastern Tibetan Plateau has undergone sustained rotation and southeastward extrusion, driven by the collision-induced uplift and deformation between the Indian and Eurasian plates. The rotation and extrusion effects have resulted in the formation of an active tectonic region characterised by large-scale strike-slip fault systems and the presence of intracontinental microplates (Tapponnier et al., 1982; Yin & Harrison, 2000; Xu et al., 2011) (Figure 1). Among these structures, the XJF and RRF serve as key strike-slip boundaries and play critical roles in the tectonic evolution and material extrusion of the southeastern Tibetan Plateau (Zhang et al., 2003; Tong et al., 2015). The intersection area of the XJF and RRF serves as the frontal zone accommodating the extrusion of the Sichuan–Yunnan Block (SYB). The XJF is blocked by the Indochina Block (ICB) and has not yet propagated southward through the RRF, which makes the intersection area the primary zone of stress accumulation, where ongoing dextral compressional motion of the SYB occurs (Wen et al., 2022; Li et al., 2024; Shao et al., 2024). The deeply incised XJF and RRF, along with secondary faults such as the Qujiang

https://doi.org/10.5194/egusphere-2025-2132
Preprint. Discussion started: 17 July 2025

Fault (QJF) and Shiping–Jianshui Fault (SJF) in this region, act as conduits for deep-circulating thermal waters and the exchange of seismic information, with thermal springs commonly found along these faults. This area experiences prolonged stress accumulation and intense tectonic deformation, accompanied by historical moderate-to-strong seismic activity (Wen et al., 2008), which makes it a critical zone for earthquake hazard monitoring. Consequently, this region is an ideal setting for investigating how variations in hydrochemical compositions respond to seismic activity.

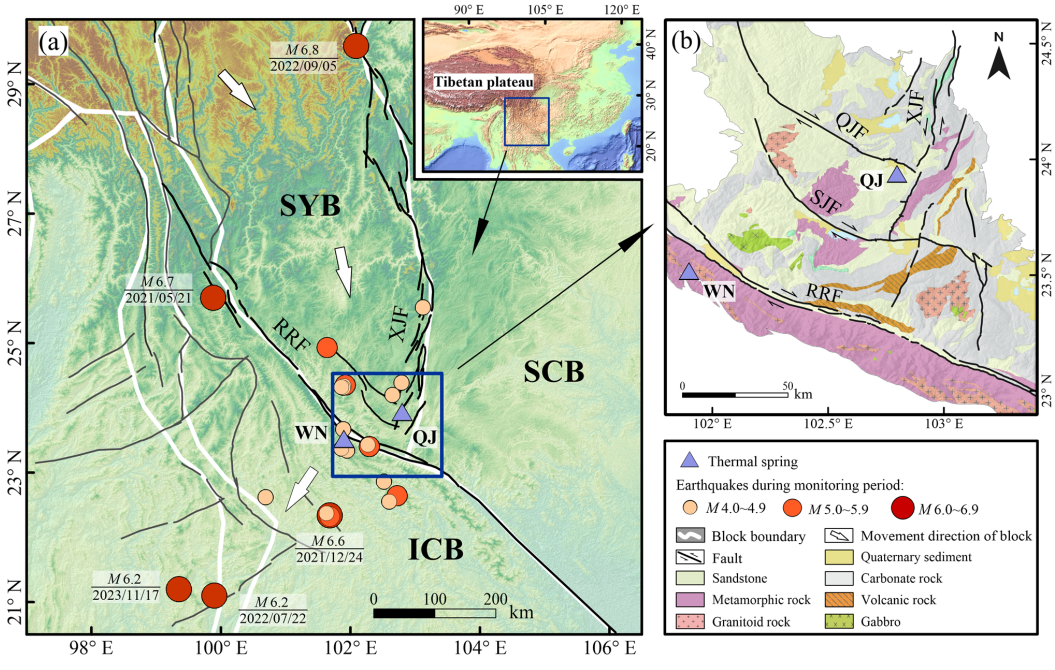

Figure 1. (a) Simplified tectonic map of the southeastern margin of the Tibetan Plateau, showing the distribution of $M \geq 4$ earthquakes during the thermal spring monitoring period. (b) Locations of continuously monitored thermal spring sites, fault distribution, and the geological map at the intersection of the Xiaojiang Fault (XJF) and Red River Fault (RRF). Earthquake catalogues are obtained from the China National Earthquake Data Center (https://data.earthquake.cn/). The tectonic divisions and active faults are sourced from Deng et al., 2002, and the geological map is adapted from Ma et al., 2002. SYB: Sichuan–Yunnan Block; ICB: Indochina Block; SCB: South

https://doi.org/10.5194/egusphere-2025-2132
Preprint. Discussion started: 17 July 2025

China Block; QJF: Qujiang Fault; SJF: Shiping–Jianshui Fault.

This study involves continuous hydrochemical monitoring at two high-temperature springs, Qujiang (QJ) and Wana (WN), located at key tectonic sites within the research area (Figure 1b). QJ is situated at the intersection of the XJF and the QJF, with sandstone as the predominant country rock. QJ is positioned at a critical location where the sinistral slip rate of the XJF decreases sharply from 8–11 mm/a to approximately 4 mm/a after crossing the QJF (Wen et al., 2011; Wang et al., 2014). WN, located along the RRF, is hosted by gneiss and mylonite and lies within a stress concentration zone, where the SYB undergoes southwestward deflection, compressing the RRF (Schoenbohm et al., 2006; Li et al., 2019; Wen et al., 2022). The two hot springs are located along the boundary faults that control the regional tectonic pattern, and their hydrochemical variations may provide sensitive indicators of changes in the earthquake preparation state within the intersection area.

3. Data and methods

3.1. Thermal spring monitoring data

The monitoring period for the QJ spring spanned from June 1, 2019, to May 21, 2024 (approximately 5 years), while the WN spring was monitored from October 3, 2021, to May 21, 2024 (approximately 2.5 years). Synchronous monitoring of hydrogen and oxygen isotopes was conducted at both springs between January 1, 2023, and February 21, 2024. All monitoring parameters for the thermal springs and their hydrochemical components were measured every three days. Water temperature, pH, and electrical conductivity (EC) were measured *in situ* using a portable multi-parameter water quality analyser (HQ40D, HACH, USA), with measurement accuracies of 0.1°C, 0.01,

https://doi.org/10.5194/egusphere-2025-2132
Preprint. Discussion started: 17 July 2025

and 1 μS/cm, respectively. Rainfall data were collected through continuous in situ monitoring using an RTP-II tri-element meteorological instrument with a resolution of 0.1 mm. Before the thermal water samples were collected, high-density polyethylene (HDPE) bottles were thoroughly rinsed three times with deionised water and twice with thermal water. Water samples were then filtered through 0.45 μm micropore membranes and stored in HDPE bottles. Samples intended for cation analysis were acidified with high-purity nitric acid. During collection, care was taken to prevent the introduction of air bubbles, and samples were immediately sealed hermetically for preservation.

The concentrations of major ions (Na^+, K^+, Ca^{2+}, Mg^{2+}, Li^+, F^-, Cl^-, SO_4^{2-}, Br^-, NO_3^-) were analysed using a Thermo Scientific Dionex Aquion IC system equipped with an AS40 autosampler, which had a detection limit of 0.01 mg/L. HCO_3^- and CO_3^{2-} concentrations were determined via standard titration procedures using a ZDJ-3D potentiometric titrator with 0.05 mol/L HCl. $\delta^{18}O$ and δ^2H values were determined using a Picarro L2140-i water isotope analyser, with precisions of 0.015 ‰ and 0.05 ‰, respectively. All analyses were conducted at the Key Laboratory of the Institute of Earthquake Forecasting, China Earthquake Administration. The monitoring data are detailed in data set S1. To ensure data accuracy, cation–anion balance error tests were performed for each sample, with all ionic deviations kept within ± 5%. The ion balance error is calculated as below:

$$ib(\%) = \frac{\sum cations - \sum anions}{\sum cations + \sum anions} \times 100 \quad (1)$$

3.2. Earthquake data collection and processing

The anomaly detection model developed in this study focused on forecasting destructive earthquakes with magnitudes (M) ≥ 4. To identify earthquakes that might influence hydrochemical

https://doi.org/10.5194/egusphere-2025-2132
Preprint. Discussion started: 17 July 2025

component variations, while excluding those unrelated to precursors, and to establish a precise correlation between changes in hydrochemical components and seismic activity, an earthquake screening method based on the preparation zone radius formula (Dobrovolsky et al., 1979) was employed:

$$R = 10^{0.43M} \quad (2)$$

where M represents the earthquake magnitude, and R denotes the radius (in km) of the earthquake preparation zone.

Earthquakes were selected as study events based on the criterion that the epicentral distance (Δ) from the thermal spring monitoring sites did not exceed the earthquake preparation zone radius (R) (Figure 1a). The QJ site was within the preparation zones of 22 $M \geq 4$ earthquakes during its monitoring period (2019/06/01–2024/05/21), while the WN site was within the preparation zones of 12 $M \geq 4$ earthquakes during its observation period (2021/10/03–2024/05/21) (Table S1). All earthquakes had focal depths ranging from 8 to 16 km, and they were classified as shallow-focus events. The earthquake catalogue was obtained from the National Earthquake Data Center of China (http://data.earthquake.cn).

Seismic moment (M_0), which directly reflects fault geometry parameters and the rigidity of the medium, accurately quantifies earthquake rupture processes and mechanical energy release. Compared with magnitude scales, the seismic moment is more suitable for analysing the seismic impact on hydrochemical component changes in thermal springs. The commonly used empirical formula for estimating seismic moment based on magnitude (Hanks & Kanamori, 1979) is as follows:

$$lgM_0 = 1.5M + 16.1 \quad (3)$$

Stress attenuates with increasing epicentral distance during the earthquake preparation process and

https://doi.org/10.5194/egusphere-2025-2132
Preprint. Discussion started: 17 July 2025

directly influences the development of thermal water seepage pathways and the intensity of water–rock interactions (Wang & Manga, 2010; Ingebritsen & Manga, 2019). To account for distance-related effects, the seismic moment requires correction using the following empirical formula (Piersanti et al., 2016):

$$M_{0cor} = M_0/\Delta^{\omega} \quad (4)$$

where ω is the weighting factor, in this study ω takes the value of 1.

3.3. Hydrochemical component time series

The geochemical behaviors of different components in thermal spring water show significant variation, with each component exhibiting distinct characteristics in terms of anomaly amplitude, temporal evolution, and precursor response sensitivity. Controlled by unique hydrogeological conditions, the hydrochemical variations of each thermal spring also display spatial differences in response to tectonic activity. To effectively extract anomalous signals, the anomaly responses of different components and springs in the study area are compared, and the algorithm's generalisability across springs is validated. This study establishes independent time series for each component at different springs (Figure 2 and S1).

https://doi.org/10.5194/egusphere-2025-2132
Preprint. Discussion started: 17 July 2025

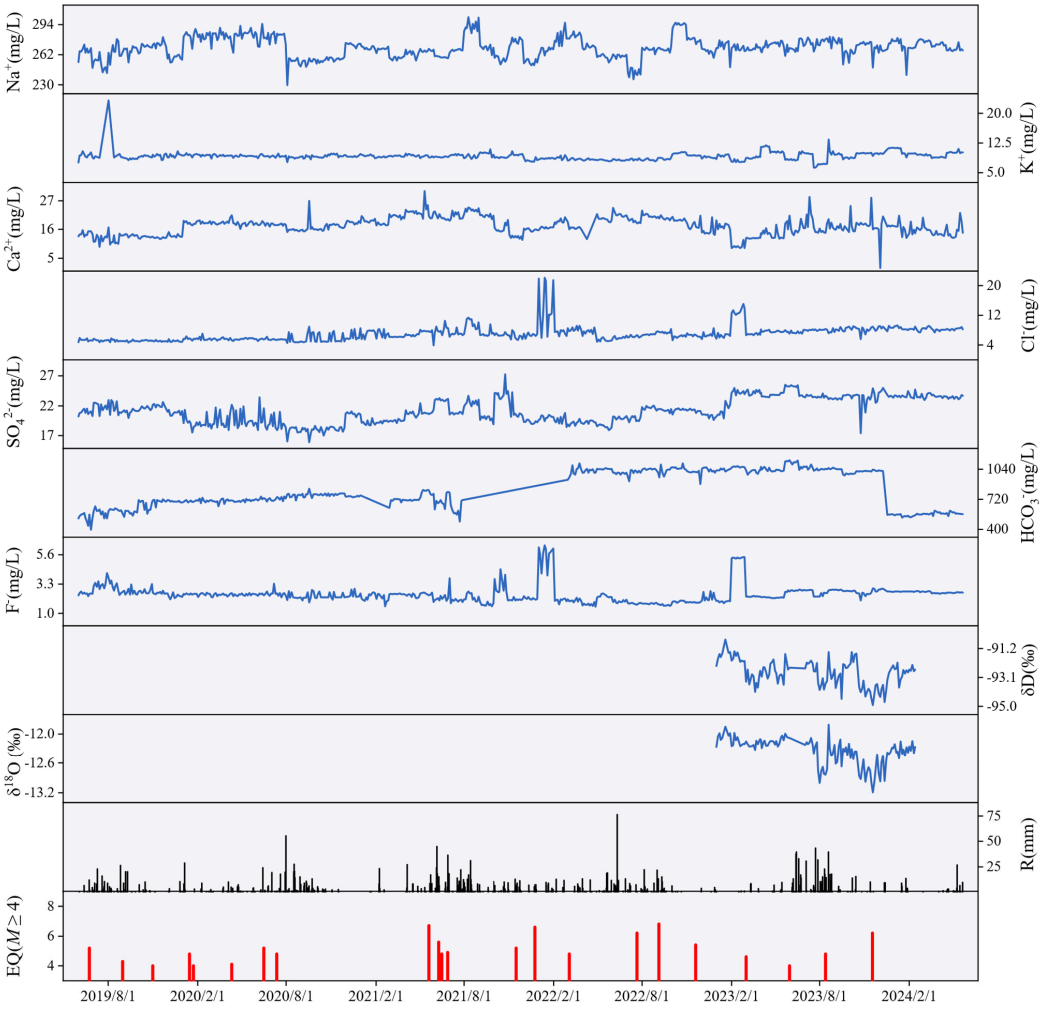

Figure 2. Time series of hydrochemical components at Qujiang spring, along with rainfall and earthquake events.

3.3.1. Data evaluation and noise removal

The dynamic variations in thermal spring ion concentrations are crucial for identifying seismic precursors. When observed data show minimal fluctuations or remain consistently below detection limits over extended periods, it becomes challenging to effectively extract hydrogeochemical anomaly signals before an earthquake. Long-term monitoring reveals that concentrations of Mg^{2+}, Br^{-}, and NO_3^{-} are extremely low and remain consistently below instrumental detection limits, without temporal

https://doi.org/10.5194/egusphere-2025-2132
Preprint. Discussion started: 17 July 2025

fluctuations, which thus limits their value for tracking seismic precursors. Consequently, Na^+, K^+, Ca^{2+}, Cl^-, SO_4^{2-}, HCO_3^-, F^-, δD, and $\delta^{18}O$ have been selected for earthquake anomaly identification owing to their consistent continuity and reliable data characteristics.

The thermal spring water in the study area originates from atmospheric precipitation recharge. It circulates deeply through faults, is heated by geothermal energy, and then discharges at the surface, with its hydrochemical composition mainly determined by the lithology of the surrounding rocks (Shao et al., 2024). Consequently, ambient temperature and atmospheric pressure at the spring outlet have a negligible effect on the hydrochemistry. However, rainfall serves not only as the primary water source but also accelerates groundwater circulation, promotes shallow infiltration, and mixes with thermal waters (Taylor et al., 2012; Hosono et al., 2020; Colman et al., 2021). This process can potentially obscure deep-seated earthquake preparatory signals carried by the thermal spring. Consequently, this study focuses on assessing the potential perturbations induced by rainfall on thermal spring hydrochemistry. Unlike temperature and pressure, rainfall causes pulsed disturbances, typically manifesting as intermittent spikes followed by extended zero-value intervals in sampling data. To suppress high-frequency noise from short-term environmental disturbances such as rainfall while preserving mid- to low-frequency tectonic signals, a 15-day backward moving average is applied to process the 3-day resolution hydrochemistry data:

$$MA(t) = \frac{1}{15}\sum_{t-14}^{t} Dr(t) \tag{5}$$

where MA is the 15-day moving average, and Dr is the daily raw data.

3.3.2. Correlation analysis

The influence of rainfall on the hydrochemical dynamics of thermal springs may exhibit a lag

https://doi.org/10.5194/egusphere-2025-2132
Preprint. Discussion started: 17 July 2025

effect, while hydrochemical precursor anomalies induced during earthquake preparation processes typically precede earthquake events. These two mechanisms exhibit a significant temporal phase difference in their perturbations to hydrochemical components. In this study, the cross-correlation function is employed to quantitatively analyse the temporal offset between the impacts of rainfall and seismic activity on thermal spring hydrochemistry. This study aims to identify the maximum correlation time offset between rainfall-hydrochemistry and precursory anomaly-main shock events via the calculation of correlation coefficients at varying lag times. The cross-correlation function is defined as:

$$CC_{xy}(k) = \frac{1}{N}\sum_{t=1}^{N-k}(x_t - \overline{x})\,(y_{t+k} - \overline{y}) \tag{6}$$

where x and y are two time series, $\overline{x}$ and $\overline{y}$ represent their sample means, N is the series length, and k denotes the lag. Considering the seasonal effects of rainfall and the response time reliability of seismic precursors, the k is set within a range of −45 to 45 days.

In the cross-correlation analysis, the denoised hydrochemical component time series (processed using a 15-day moving average) are correlated with both the rainfall time series and the distance-corrected M_0 time series. This analysis aims to evaluate the effectiveness of the moving-average method in filtering out rainfall-induced interference by assessing the correlation intensity between the denoised hydrochemical time series and rainfall. At the same time, the analysis verifies potential temporal linkages between the denoised hydrochemical components and regional seismic moment release.

https://doi.org/10.5194/egusphere-2025-2132
Preprint. Discussion started: 17 July 2025

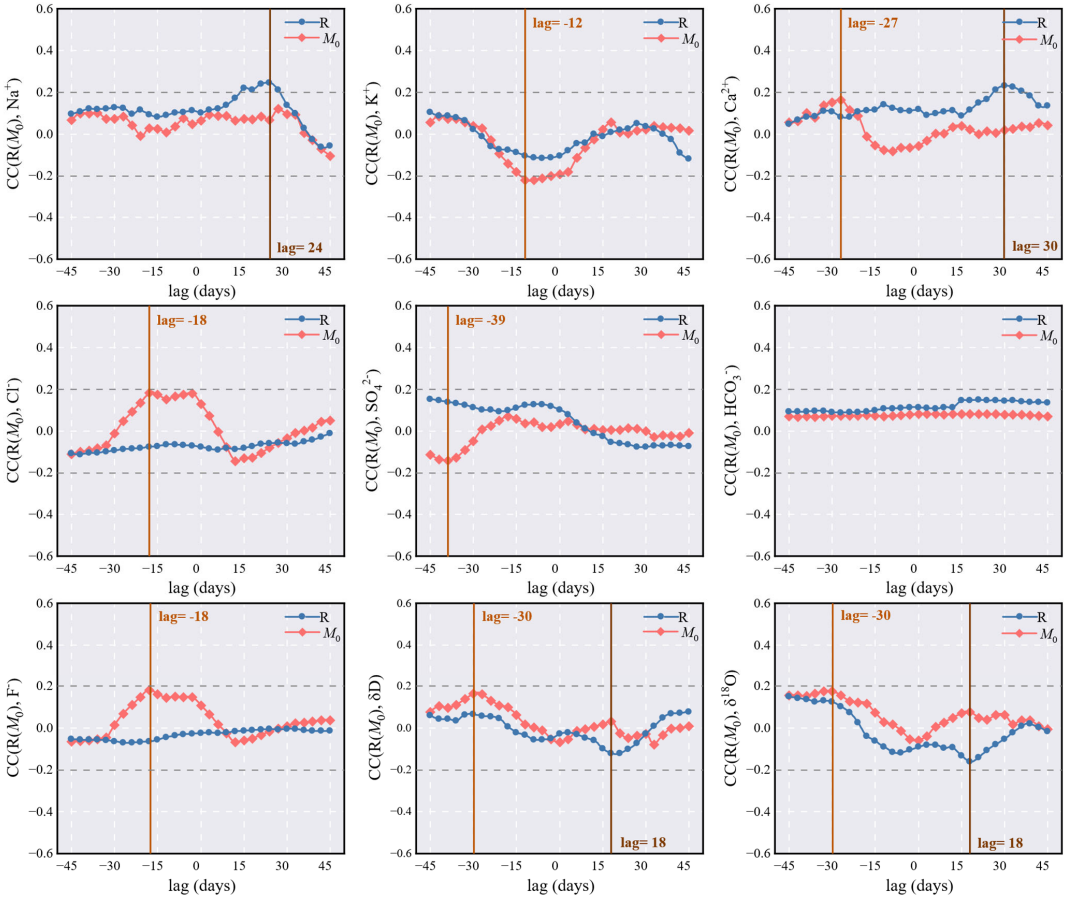

Figure 3. Cross-correlation function analysis of the 15-day moving average time series of hydrochemical components during stable isotope monitoring, with rainfall and distance-corrected seismic moment.

The results of the cross-correlation analysis (Figure 3) show weak correlations (blue dotted lines) between rainfall events and the 15-day moving average hydrochemical component time series, with correlation coefficients approximately within ± 0.2. This result indicates that the moving average treatment effectively mitigates rainfall-induced noise. Notably, Na^+, Ca^{2+}, δD, and $\delta^{18}O$ exhibit minor response peaks at lags of 18–30 days, suggesting that certain impacts on these components persist 15 to 30 days after rainfall. Similarly, the correlations between the distance-corrected M_0 and the denoised

https://doi.org/10.5194/egusphere-2025-2132
Preprint. Discussion started: 17 July 2025

hydrochemical component time series (red dotted lines) remain low (around ± 0.2). However, K^+, Ca^{2+}, Cl^-, SO_4^{2-}, F^-, δD, and $\delta^{18}O$ exhibit weak response peaks at lags of −39 to −12 days, with varying peak directions for each component. This observation suggests that seismic activity (12–39 days before seismic moment release) may influence hydrochemical components, causing their concentrations to fluctuate (either increasing, decreasing, or remaining stable) owing to different geochemical mechanisms.

3.4. Detection algorithms

3.4.1. BCP analysis

The correlation analysis results indicate that changes in environmental parameters have little to no significant influence on denoised hydrochemical components, or their effects were slow processes. Consequently, these component time series appear to follow specific distribution patterns. However, since earthquake events are stochastic and hydrochemical anomalies (i.e., change points) emerge during the pre-earthquake period without a known rupture time, continuous hydrochemical monitoring data exhibit non-stationary variations. Therefore, BCP analysis is applied to effectively extract anomalous signals from these component time series.

To detect change points in pre-seismic hydrochemical component time series and verify their correspondence with earthquakes for forecasting future earthquake occurrences, the BCP analysis algorithm, which is developed for Earth climate systems (Ruggieri, 2012) to the 15-day moving average time series of all component concentrations from QJ and WN, is applied to this study. The analysis produces Bayesian predictive model curves, change point locations, and posterior

https://doi.org/10.5194/egusphere-2025-2132
Preprint. Discussion started: 17 July 2025

292 probabilities for each component. The posterior probabilities represent the likelihood of change point
293 occurrences in the predictive models, with probability peaks indicating the most likely timings of
294 change points.

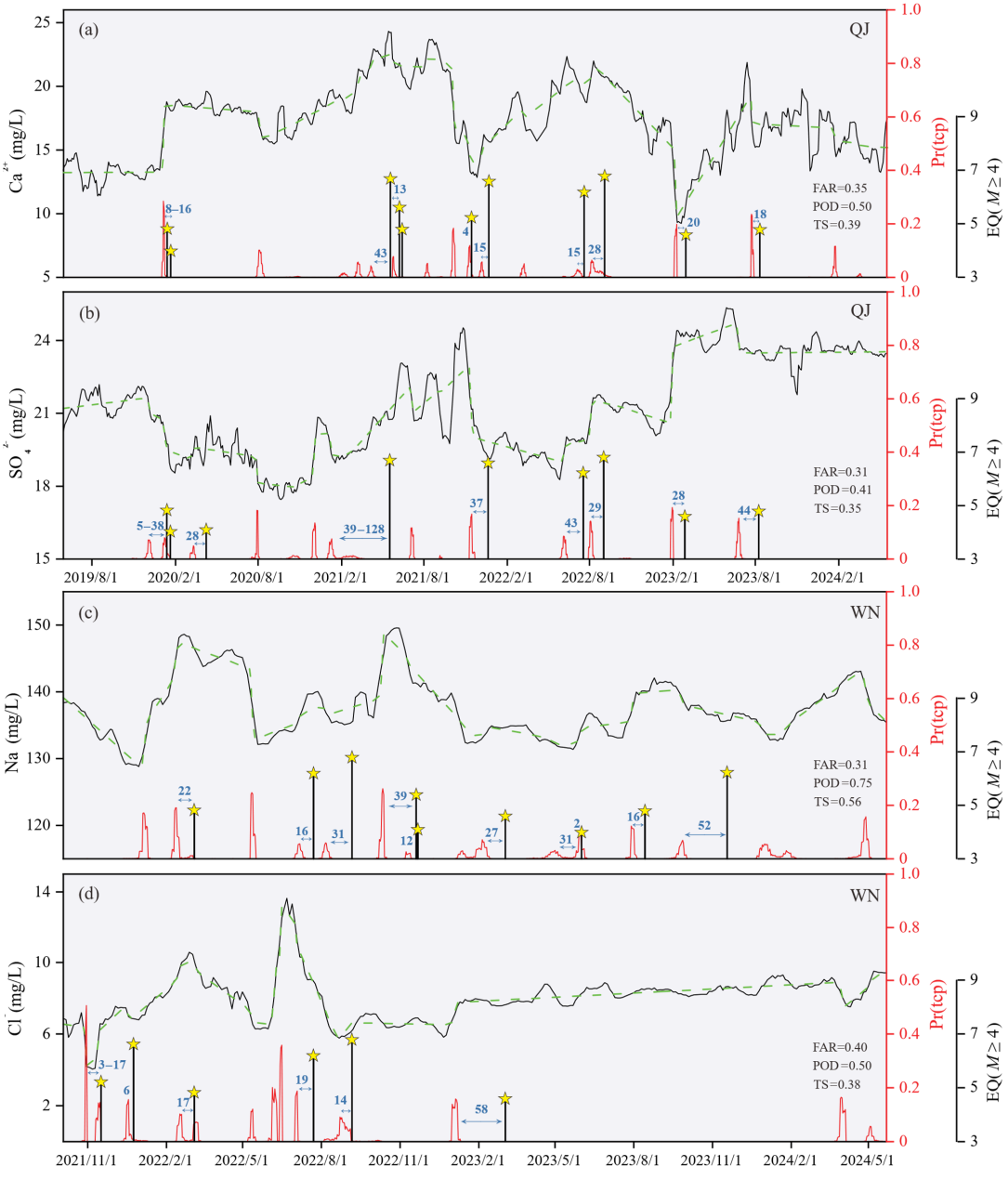

295

https://doi.org/10.5194/egusphere-2025-2132
Preprint. Discussion started: 17 July 2025

Figure 4. Anomaly detection results from the Bayesian change point (BCP) analysis applied to hydrochemical component time series. The black solid line represents the component concentration after 15-day moving averaging. The green dashed line indicates the forecasting model of the BCP algorithm. The red solid line shows the posterior probability of change points. Yellow stars mark earthquake events. The false alarm rate (FAR), probability of detection (POD), and threat score (TS) are evaluation metrics; further details are provided later.

The results show that change points are successfully detected in all component time series from both thermal springs (Figure 4). For example, before the *M*6.6 earthquake on December 24, 2021, the posterior probability for a Ca^{2+} change point at QJ was 0.06 at 15 days before the earthquake, while SO_4^{2-} exhibited a posterior probability of 0.17 at 37 days before the earthquake. Similarly, before the *M*5.2 earthquake on November 16, 2021, Cl^- at WN showed posterior probabilities for change points of 0.15 and 0.51 at 3 and 17 days before the earthquake, respectively. Notably, the timing and posterior probabilities of change points exhibit significant uncertainty, which reflects the complexity of factors influencing hydrochemical component variations. These factors include inhomogeneity in stress accumulation, the structural complexity of fault and aquifer systems, modulation by deep gas degassing, and the mixing effects of multi-source fluids (Skelton et al., 2014; Kim et al., 2019; Hosono et al., 2020). Although earthquakes result from the coupling of multiple factors, most change points are identified within 45 days preceding the earthquakes. This observation suggests that component concentration changes are sensitive to earthquake preparation processes and do occur before earthquakes, which provides critical empirical support for anomaly detection algorithm models.

The BCP analysis algorithm for anomaly detection also has limitations. Compared with the Na^+ detection results at WN, the Cl^- time series produces two false positives for 2022 and misses three

https://doi.org/10.5194/egusphere-2025-2132
Preprint. Discussion started: 17 July 2025

earthquakes for 2023 (Figure 4c, d). This result suggests that the analysis requires a longer time series and is highly sensitive to prior distribution settings. In practice, identifying the locations and probabilities of earthquake-induced change points in hydrochemical component time series is challenging. Larger-amplitude component changes often overshadow smaller-amplitude variations, which makes the latter difficult to detect and more prone to missed detections or false positives. Additionally, most BCP methods have a fundamental limitation: they inherently perform retrospective analysis on complete time series. Specifically, identifying a change point at time t_i relies on data collected after t_i ($t > t_i$), which makes real-time, forward earthquake forecasting unfeasible with short-term data sequences (Piersanti et al., 2016).

3.4.2. Anomaly detection model

According to the results of the BCP analysis, change-point detection for earthquake forecasting should be viewed as a supplementary approach. This study enhances the real-time anomaly detection algorithm for soil radon concentration time series (Piersanti et al., 2016; Soldati et al., 2020) and applies it to hydrochemical multicomponent time series (Na^+, Cl^-, SO_4^{2-}, δD, $\delta^{18}O$, etc.). The aim is to establish an anomaly detection model within a multi-parameter feature space to explore potential correlations between hydrochemical component variations and major earthquakes. This study modifies the algorithmic workflow to a backward processing mode and enables real-time forward forecasting. In the study, evaluation metrics for parameter optimisation are introduced and a seismic response time threshold parameter, which accounts for local geological conditions is incorporated. The detection model processes hydrochemical component time series and confirms earthquake catalogues, fitting optimal parameters based on the evaluation metrics to generate the best anomaly detection parameter

https://doi.org/10.5194/egusphere-2025-2132
Preprint. Discussion started: 17 July 2025

combinations for each component. The optimised model performs online, point-by-point data processing for real-time monitoring. When real-time hydrochemical data deviates from the threshold, the model triggers an alarm to predict earthquakes, which enhances forecasting accuracy through multicomponent collaboration (Figure 5). The model improves in three ways: 1) the model incorporates a multi-parameter collaborative verification mechanism that reduces environmental noise interference; 2) the model identifies components with superior anomaly detection performance; 3) the model analyses anomaly intensity based on the number of components detecting anomalies for the same earthquake, thereby improving detection accuracy and reducing false positives and missed alarms.

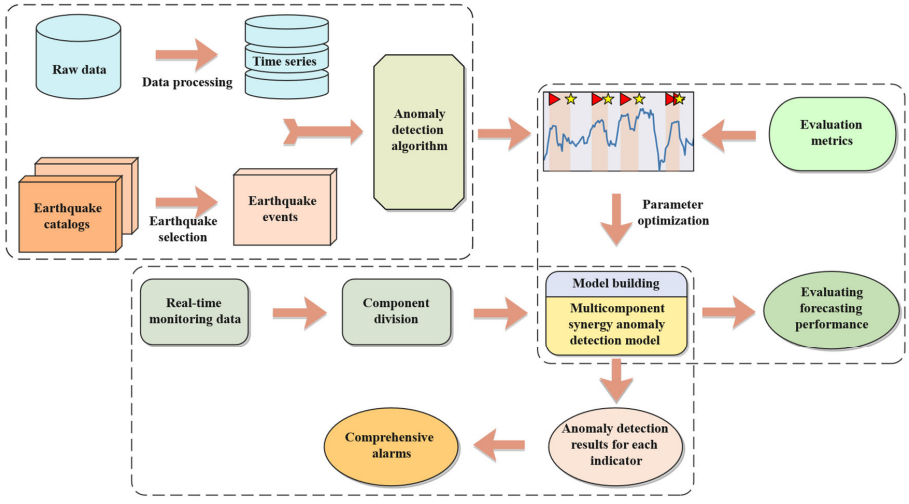

Figure 5. Framework of the hydrochemical multicomponent synergy anomaly detection model.

The improved detection algorithm procedure (Figure S2) is as follows: Real-time monitoring data for each component from day i are loaded. If the daily value on day i−p2 exceeds p1 times the 15-day moving average on day i−p2−1, and simultaneously, the 15-day moving average on day i surpasses p3 times that on day i−p2, the system triggers an alarm on day i. This alarm is considered a successful

https://doi.org/10.5194/egusphere-2025-2132
Preprint. Discussion started: 17 July 2025

early warning if an $M \geq 4$ earthquake occurs within I + T_{th}. After an earthquake, new parameters p1' = p4 × p1 and p3' = p4 × p3 are used for a period of p5^M (where M is the magnitude). If subsequent earthquakes occur within this period, the post-earthquake time is calculated based on the maximum magnitude. If no $M \geq 4$ earthquakes occur during this interval, parameters p1 and p3 automatically revert to their initial values. The algorithm incorporates five adjustable parameters (p1–p5) and a seismic response time threshold (T_{th}), with p1, p3, and T_{th} being key parameters.

When thermal water is subjected to external disturbances (e.g., contamination or anthropogenic inputs), particularly the dissolution of a single compound, variations in hydrochemical ion concentrations generally follow the charge balance principle, often resulting in synchronous changes in paired cations and anions. To minimise the impact of uncertain interference and improve program efficiency, reliable warning signals should be defined by concurrent alarms from at least three hydrochemical components. The intensity of the anomaly increases with the number of components triggering simultaneous alarms.

3.4.3. Evaluation metrics

Given that earthquake forecasting research focuses on evaluating algorithms' ability to identify low-probability earthquake events, this study employs four evaluation metrics based on the number of correct alarms (NA), false alarms (NB), and missed alarms (NC).

False alarm rate (FAR): This measures the proportion of non-earthquake events incorrectly classified as earthquake events, relative to the total number of warning instances.

$$FAR = NB/(NA + NB) \quad (7)$$

Missed alarm rate (MAR): The proportion of earthquakes that are not detected relative to the total

https://doi.org/10.5194/egusphere-2025-2132
Preprint. Discussion started: 17 July 2025

number of earthquake events, indicating the risk of failing to identify such events.

$$MAR = NC/(NA + NC) \quad (8)$$

Probability of detection (POD): The proportion of correctly identified earthquake events out of all earthquake events, assessing the model's ability to detect these events.

$$POD = NA/(NA + NC) \quad (9)$$

Threat score (TS): This reflects the accuracy of the forecast, ranging from 0 (complete mismatch) to 1 (perfect match) with actual events.

$$TS = NA/(NA + NB + NC) \quad (10)$$

This metric system allows for a more accurate evaluation of the model's forecasting performance in handling imbalanced data through multi-dimensional quantitative analysis.

4. Results and discussion

4.1. Hydrochemistry

The average water temperature at QJ is approximately 60°C, with a pH of 7.5 and an EC of 1148 μS/cm, while WN has a higher temperature of 80°C, a pH of 7.9, and a lower EC of 579 μS/cm. Both QJ (sandstone) and WN (mylonite, gneiss, etc.) exhibit similar hydrochemical types (HCO_3-Na), owing to the comparable lithology of the surrounding rocks. The $\delta^{18}O$ values at QJ range from −13.19‰ to −11.81‰, while the δD values range from −94.93‰ to −90.59‰. At WN, the $\delta^{18}O$ values range from −13.22‰ to −12.01‰, and the δD values range from −91.26‰ to −88.09‰. The narrow fluctuation range of stable isotopes in both thermal springs, coupled with their proximity to the local and global meteoric water lines (Figure S3), suggests that the thermal spring water originates from

https://doi.org/10.5194/egusphere-2025-2132
Preprint. Discussion started: 17 July 2025

atmospheric precipitation. Overall, the two springs exhibit similar hydrochemical characteristics, which minimises the impact of compositional differences on the evaluation of algorithm effectiveness across the different springs. For detailed hydrochemical ion concentrations and isotope values, please refer to the supplementary materials.

4.2. Model parameters

4.2.1. Seismic response time threshold

The anomaly detection model in this study establishes forecasting rules based on the temporal correlation between precursor anomalies and earthquake events. The seismic response time threshold (T_{th}) plays a key role in determining both forecasting performance and practical value. T_{th} is defined as the maximum allowable time interval between anomaly detection and earthquake occurrence. This threshold is a critical parameter that balances accuracy and timeliness. Increasing T_{th} expands the monitoring window and captures more potentially correlated abnormal signals, but it significantly reduces the time resolution of forecasting. Conversely, decreasing T_{th} improves temporal precision but may risk omitting valid precursor signals owing to shorter observation periods.

To improve the accuracy of the anomaly detection model in predicting earthquake timing, the nonlinear effects of T_{th} on predictive performance are systematically explored via an incremental increase of T_{th} from 5 to 70 days in 5-day steps. This increase identifies key inflection points during threshold optimisation (Figure S4). As T_{th} increases from 5 to 45 days, model performance improves considerably, with both TS and POD rising rapidly, while FAR gradually decreases. This improvement results from the extended monitoring windows, which better capture the association between

https://doi.org/10.5194/egusphere-2025-2132
Preprint. Discussion started: 17 July 2025

anomalies and seismic activities. Notably, the evaluation metrics reveal a turning point at the 45-day threshold. Beyond 45 days, the trends in TS, POD, and FAR plateaus, with minimal variation. This result is consistent with the finding that maximum cross-correlations between M_0 and hydrochemical components (Cl^-, SO_4^{2-}, δD) occur within 45 days before the earthquake (Figure 3) and that BCP analysis detects most change points emerging within 45 days of pre-earthquake events (Figure 4). Collectively, these results jointly define 45 days as the optimal response time threshold for hydrochemical precursors to seismic activities in the study area.

4.2.2. Free parameters

The parameter optimisation process involves quantitatively aligning observed hydrochemical data with seismic precursor anomalies. Among the five adjustable parameters (p1–p5) in the detection model, the key regulatory parameters p1 and p3 represent multiples of the sliding window values. This study focuses on p1 and p3 to examine the influence of the optimisation of these parameters on the performance of the anomaly detection model. For optimisation involving ion concentration data, the model applies parameter values ranging from 1.00 to 1.20 in steps of 0.01. For optimisation involving isotopic data, which exhibit minor fluctuations, the model applies parameter values ranging from 0.985 to 1.015, with a step increment of 0.001. Model performance is then evaluated using TS. Figure 6 shows the variations in the TS under different values of p1 and p3. When p1 and p3 are small, the model becomes overly sensitive to background noise, detecting more non-seismic signals. This effect leads to an increase in the FAR and a decrease in TS. As p1 and p3 increase, TS improves. However, when the parameters become excessively large, surpassing the actual seismic anomaly thresholds, the MAR rises sharply, which causes TS to drop below 0.35. The optimal parameter combinations for each

https://doi.org/10.5194/egusphere-2025-2132
Preprint. Discussion started: 17 July 2025

436 hydrochemical component are identified at the TS peak inflection points (marked by yellow circles).
437 According to this method, the complete set of model parameters for all hydrochemical components at
438 QJ and WN is provided in Table S2.

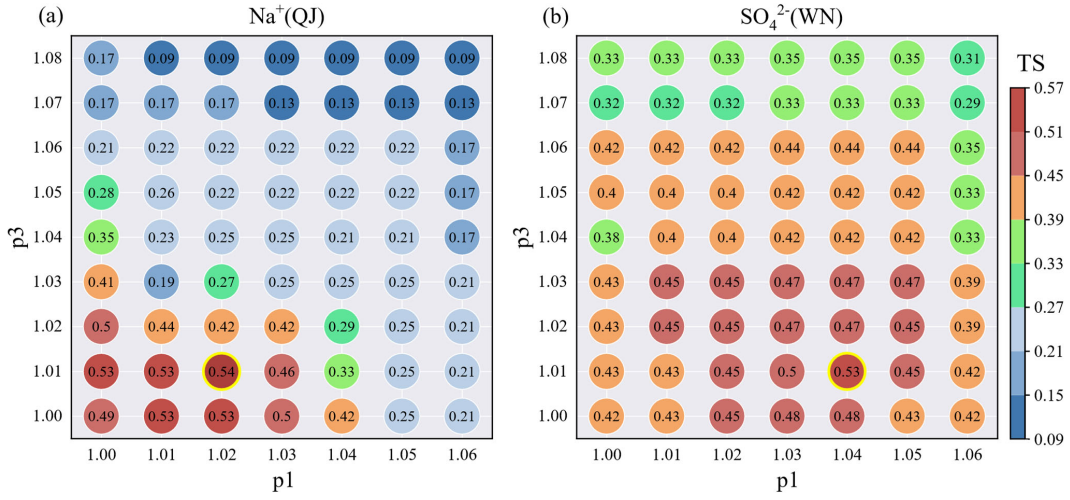

439

440 Figure 6. Effect of parameters on model performance. TS varies with changes in p1 and p3 (the main free
441 parameters p1 and p3 are used as examples). The yellow circle highlights the TS value corresponding to the optimal
442 combination of p1 and p3.

443 The parameter optimisation results reveal notable differences in the optimal p1 and p3
444 combinations for different hydrochemical components. Hydrochemical anomalies preceding
445 earthquakes in many regions are typically caused by the combined action of multiple mechanisms
446 (Skelton et al., 2014; Kim et al., 2019; Hosono & Masaki, 2020). Furthermore, owing to significant
447 variations in the geochemical behavior of different hydrochemical components, components within
448 the same thermal spring often exhibit diverse response patterns to the same earthquake. These patterns
449 may include asynchronous variations (increase/decrease/stability) and considerable discrepancies in
450 the magnitude of change (Shi et al., 2020; Wang et al., 2021; Tian et al., 2023). Therefore, optimising

https://doi.org/10.5194/egusphere-2025-2132
Preprint. Discussion started: 17 July 2025

parameter combinations to create customised anomaly detection models for specific hydrochemical components at designated observation points is the key approach in this study to enhance the model's ability to detect seismic precursor information.

4.3. Evaluation of forecasting performance

Figures 7 and 8 present the 15-day moving average time series of hydrochemical components, anomaly detection results, and earthquake events for the anomaly detection model at QJ and WN. For each component, the model successfully identifies varying numbers of pre-earthquake anomalies and triggered warnings. The model activates comprehensive alarms when anomalies are detected in three or more components simultaneously. At QJ, the model provides 21 effective warnings for 22 earthquake events (POD = 0.95), with 8 false alarms (FAR = 0.28) and a TS of 0.70. At WN, the model generates 10 accurate warnings for 12 events (POD = 0.83), 5 false alarms (FAR = 0.33), and a TS of 0.59. Compared with the single-component anomaly detection results, the multi-component joint warning results exhibit higher TS values (Figures 7, 8, 9). This observation demonstrates that multicomponent collaboration mitigates the effects of geochemical behavior differences among components, reduces environmental interference on individual ions/ion pairs, and consequently enhances the accuracy of the anomaly detection model. Zhu et al. (2024) comprehensively evaluated the anomaly detection performance of several machine learning algorithms using 2.5 years of hydrochemical data from the southeast coast of China. The best-performing local outlier factor algorithm achieved an R-score of about 0.6, POD of about 0.7, and FAR of about 0.15. The improved anomaly detection model demonstrates comparable performance, which confirms its effectiveness.

https://doi.org/10.5194/egusphere-2025-2132
Preprint. Discussion started: 17 July 2025

The results from the anomaly detection model and BCP analysis are mutually corroborative; however, the anomaly detection model exhibits superior sensitivity in processing nonlinear time series data. Taking QJ as an example, the model achieves POD values of 0.70 and 0.59 for Ca^{2+} and SO_4^{2-} detection results, respectively (Figures 4 and 7), which represents significant improvements over the BCP analysis results (0.50 and 0.41). The model is also capable of accurately detecting subtle anomalies that the BCP analysis may miss.

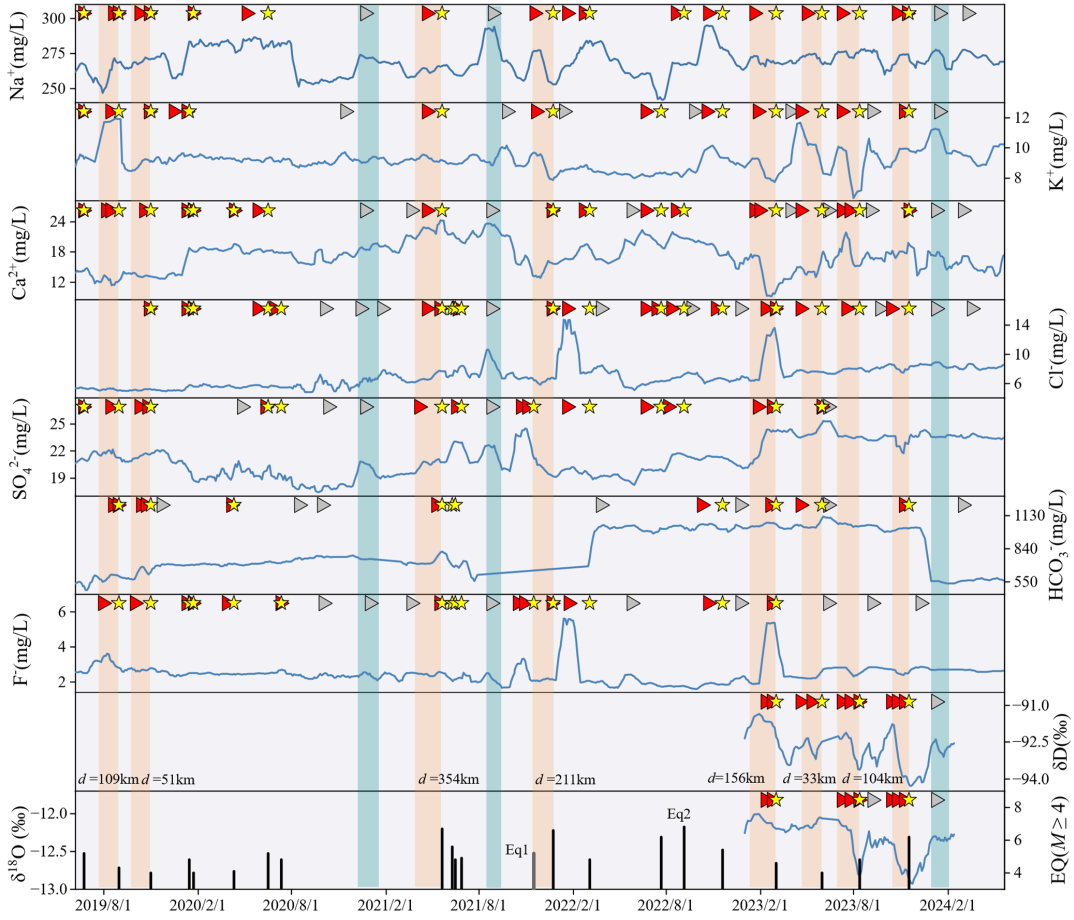

Figure 7. Results of the anomaly detection model applied to hydrochemical component time series from Qujiang spring. The blue curve represents the hydrochemical component time series after a 15-day moving average. Red and

https://doi.org/10.5194/egusphere-2025-2132
Preprint. Discussion started: 17 July 2025

gray triangles indicate accurate alarms and false alarms, respectively. Yellow stars mark successfully reported earthquakes. Black and gray vertical bars show detected and missed earthquakes based on the algorithm's comprehensive alarm (triggered by ≥ 3 components), respectively. Orange-red boxes highlight synchronous successful alarms triggered by six or more components. Grayish-blue boxes mark synchronous false alarms triggered by five or more components.

Owing to variations in the geochemical behaviors of hydrochemical components, their response patterns and magnitudes to earthquakes differ. Although the mechanisms behind these differences have not yet reached academic consensus, this study aims to identify effective strong earthquake prediction indicators applicable to the study area through anomaly detection model results. A comparison of the TS values of each component's warning results in QJ and WN (Figure 9) reveals that in the two thermal springs of the study area, the TS values for Na^+, Ca^{2+}, Cl^-, SO_4^{2-}, δD, and $\delta^{18}O$ detection (around 0.50) are relatively high. This observation suggests that these components can serve as sensitive indicators for strong earthquake forecasting in the study area. In general, QJ in the study area exhibits a more sensitive response to earthquakes. In addition, the anomalies are categorised into multiple consecutive anomalies and single anomalies (Figures 7 and 8). This phenomenon is more pronounced in the stable isotope time series, likely because isotopic changes are more sensitive and tend to trigger multiple warning signals before an earthquake.

https://doi.org/10.5194/egusphere-2025-2132
Preprint. Discussion started: 17 July 2025

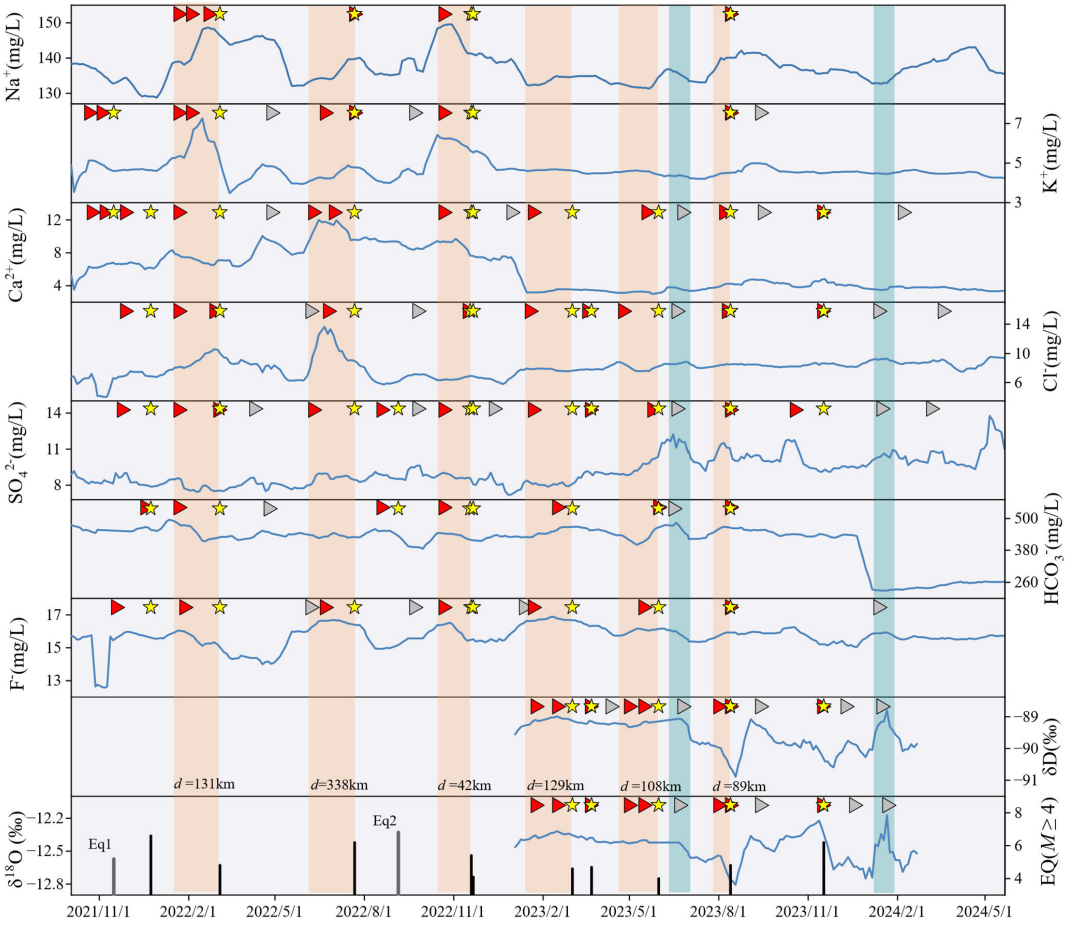

Figure 8. Results of the anomaly detection model applied to hydrochemical component time series from Wana spring. The same notes as above for Figure 7.

Among the earthquakes for which the earthquake preparation zone covers both thermal springs, only two earthquakes (represented by gray vertical bars in Figures 7 and 8) fail to induce multicomponent anomalies prior to the earthquake. Earthquake Eq1 causes no synchronous anomalies at either spring, which suggests that Eq1 has a limited impact on regional tectonic activity. For Eq2 (epicentral distance > 600 km), WN shows no alarm response, while QJ reacts effectively. This discrepancy is likely related to WN's location on the eastern boundary of the SYB, where stress

https://doi.org/10.5194/egusphere-2025-2132
Preprint. Discussion started: 17 July 2025

accumulation mainly affects QJ, which is also located on the eastern border. The muted response in WN likely results from the blocking effects of the RRF (Li et al., 2024; Shao et al., 2024). The similar abnormal response sensitivity of different springs to the same earthquake demonstrates regional-scale hydrochemical impacts from earthquake preparation and confirms the stable and reliable performance of the anomaly detection model.

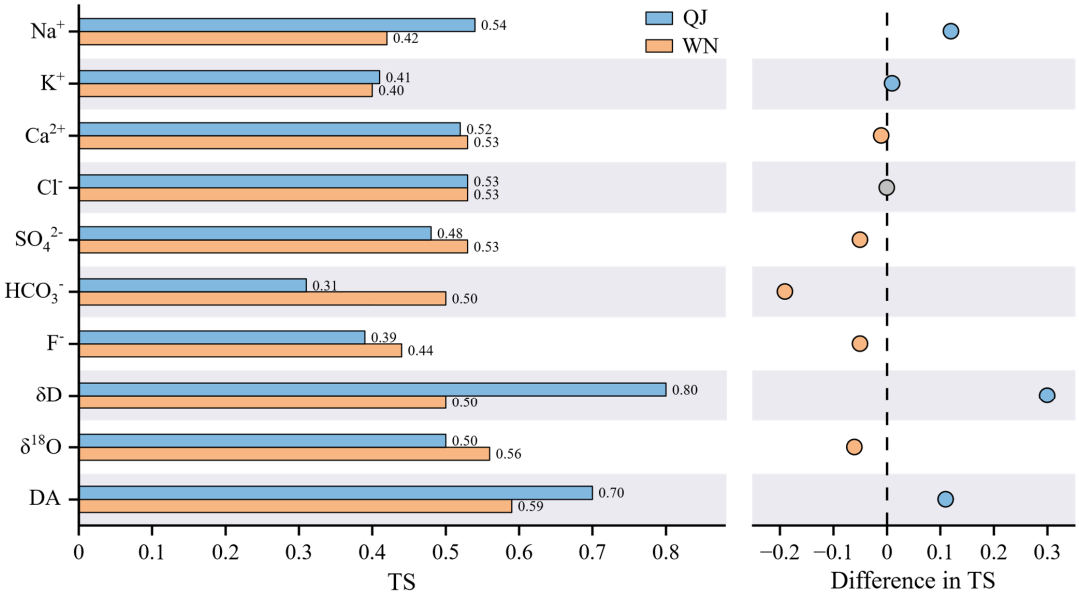

Figure 9. TS values of anomaly detection model results for hydrochemical components. DA denotes comprehensive alarms triggered by the model.

In Figures 7 and 8, the orange-red boxes represent model results of successfully predicted earthquakes, identified through synchronised anomalies in six or more hydrochemical components. The width of the boxes, which indicates the interval between the appearance of anomalies and earthquake occurrence, shows no clear correlation with magnitude or epicentral distance. This observation underscores the complex dynamic mechanisms and regional structural differences

https://doi.org/10.5194/egusphere-2025-2132
Preprint. Discussion started: 17 July 2025

involved in the earthquake preparation process, with anomalies often arising from the combined effects of multiple mechanisms (Thomas, 1988). Spatially, the number of hydrochemical components exhibiting synchronous anomalies correlates with earthquake magnitude and epicentral distance. Earthquakes that induce synchronous anomalies in six or more hydrochemical components have epicentral distances within 150 km for earthquakes with magnitudes less than 6.0 ($M < 6.0$), while this distance extends to approximately 450 km for earthquakes with magnitudes greater than or equal to 6.0 ($M \geq 6.0$). Although it is difficult to quantify the exact impact of magnitude and distance on the number of components exhibiting synchronous anomalies, as magnitude increases or distance decreases, the number of components with synchronous anomalies detected by the model tends to increase. This trend aligns with the positive correlation between the scale of earthquake energy release and the number of anomalies, as confirmed by the hydrochemical monitoring results (Li et al., 2022). Therefore, a significant relationship exists between the temporal variation of hydrochemical components and earthquakes in the study area. The number of components exhibiting synchronous anomalies can be used as an effective criterion for determining alarm intensity, with higher intensity generally corresponding to larger earthquake magnitudes or shorter epicentral distances.

Furthermore, this study reveals that hot springs closer to the epicenter tend to exhibit a greater number of components with synchronous anomalies during the same earthquake. Pre-earthquake hydrochemical anomalies generally manifest on a regional scale, which means different thermal springs can not only validate each other in terms of anomaly timing for forecasting purposes but also help identify the closest springs to the epicenter based on the number of synchronous anomalous components. This approach aids in defining potential earthquake preparation zones. According to this

https://doi.org/10.5194/egusphere-2025-2132
Preprint. Discussion started: 17 July 2025

approach, a dense thermal spring monitoring network provides more opportunities for spatial earthquake forecasting.

4.4. Limitations and prospects

This study focuses on evaluating the performance of anomaly detection models in predicting the timing of earthquakes with magnitudes ≥ 4. One potential cause of false alarms could be anomalous fluctuations in hydrochemical components triggered by seismic activities with magnitudes < 4 in areas near thermal springs. Four days after the second synchronised false alarm involving five components (Figure 7, grayish-blue boxes), an *M*2.6 earthquake occurred 3 km from QJ. This occurrence suggests that high-frequency false alarms may not solely result from non-seismic fluid anomalies, but could also reflect the model's limited ability to distinguish anomalies caused by microseisms. According to this finding, it is recommended to establish observation station networks and optimise algorithms to enable hierarchical alarm systems. Approximately 30 days after the last multicomponent synchronised false alarms at the two thermal springs (Figures 7 and 8), an *M*4.1 earthquake occurred, with an epicenter located outside the radius of the earthquake preparation zone. Current earthquake screening criteria assume an isotropic underground structure; however, the algorithm requires tailored optimisation based on the specific geological background in practical applications. Additionally, the model demonstrates limited adaptability to changes in data trends, highlighting the need for periodic parameter re-optimisation. While the model is constructed using major elements and stable isotopic indicators in thermal waters, future research should also consider the potential associations between other hydrochemical components, such as trace elements, and seismic activity.

https://doi.org/10.5194/egusphere-2025-2132
Preprint. Discussion started: 17 July 2025

5. Conclusions

A multicomponent synergistic anomaly detection model is developed using five years of continuous hydrochemical monitoring data to enable real-time forecasting of $M \geq 4$ earthquakes in the study area. Model parameters are optimised for each component, and their impact on anomaly detection performance is evaluated to identify applicable hydrochemical indicators for strong earthquake forecasting. The results of the multicomponent synergy anomaly detection reveal a clear connection between hydrochemical variations and seismic activity, offer valuable insights, and establish a new paradigm for precursor identification in earthquake forecasting. The main findings are summarised as follows:

1. A 45-day response time threshold for hydrochemical components to $M \geq 4$ earthquakes is established as the optimal period for capturing key hydrochemical precursors for short-term earthquake forecasting. Tailored model parameters for specific hydrochemical components account for their differences in response characteristics to seismic activity and significantly enhance the model's performance and adaptability.
2. The anomaly detection model demonstrates reliable real-time anomaly detection capabilities and identifies Na, Ca^{2+}, Cl^{-}, SO_4^{2-}, δD, and $\delta^{18}O$ as effective indicators for strong earthquake forecasting, with δD and $\delta^{18}O$ exhibiting higher sensitivity to seismic activity.
3. The newly proposed multi-parameter synergy alarm mechanism for hydrochemistry overcomes the limitations of single-parameter methods and significantly improves the model's overall performance in earthquake forecasting. The number of hydrochemical components with

https://doi.org/10.5194/egusphere-2025-2132
Preprint. Discussion started: 17 July 2025

synchronous anomalies provides a reliable criterion for determining alarm intensity, with higher intensity typically correlating to larger earthquake magnitudes or shorter epicentral distances. A dense thermal spring monitoring network can facilitate cross-verification across multiple sites for time-based forecasting and offer enhanced capabilities for spatial forecasting.

Acknowledgments

This work was jointly supported by National Key Research and Development Project (No. 2023YFC3012005-1), National Natural Science Foundation of China (No. 42073063), Special Fund of the Institute of Earthquake Forecasting, China Earthquake Administration (No. CEAIEF20230301), Deep Earth Probe and Mineral Resources Exploration National Science and Technology Major Project (No. 2024ZD1000503). This work is a contribution to IGCP Project 724.

Declaration of interest

The authors declare that they have no known competing financial interests or personal relationships that could have appeared to influence the work reported in this paper.

Data availability

The continuous monitoring data from thermal springs can be found at Mendeley Data, Version 1 (https://10.17632/xkd75cyfmb.1).

https://doi.org/10.5194/egusphere-2025-2132
Preprint. Discussion started: 17 July 2025

References

Barbieri, M., Franchini, S., Barberio, M. D., Billi, A., Boschetti, T., Giansante, L., Gori, F., Jonsson, S., Petitta, M., Skelton, A., and Stockmann, G.: Changes in groundwater trace element concentrations before seismic and volcanic activities in Iceland during 2010-2018, Sci Total Environ, 793, 148635, https://doi.org/10.1016/j.scitotenv.2021.148635, 2021.

Castellana, L., and Biagi, P.: Detection of hydrogeochemical seismic precursors by a statistical learning model, Natural Hazards and Earth System Sciences, 8(6), 1207-1216, 2008.

Chaudhuri, H., Bari, W., Iqbal, N., Bhandari, R. K., Ghose, D., Sen, P., and Sinha, B.: Long range gas-geochemical anomalies of a remote earthquake recorded simultaneously at distant monitoring stations in India, Geochemical Journal, 45(2), 137-156, 2011.

Chen Y.: Earthquake prediction: Retrospect and prospect (in Chinese), Science China Series D: Earth Sciences, 39(12), 1633-1658, 2009.

Colman, D. R., Lindsay, M. R., Harnish, A., Bilbrey, E. M., Amenabar, M. J., Selensky, M. J., Fecteau, K. M., Debes, R. V., 2nd, Stott, M. B., Shock, E. L., and Boyd, E. S.: Seasonal hydrologic and geologic forcing drive hot spring geochemistry and microbial biodiversity, Environ Microbiol, 23(7), 4034-4053, https://doi.org/10.1111/1462-2920.15617, 2021.

Deng, Q., Zhang, P., Ran, Y., Yang, X., Min, W., and Chu, Q.: Basic characteristics of active tectonics of China (in Chinese), Science China Series D: Earth Sciences, 32(12), 1020-1030+1057, 2002.

Di Matteo, L., Dragoni, W., Azzaro, S., Pauselli, C., Porreca, M., Bellina, G., and Cardaci, W.: Effects of earthquakes on the discharge of groundwater systems: The case of the 2016 seismic sequence in the Central Apennines, Italy, Journal of Hydrology, 583, https://doi.org/10.1016/j.jhydrol.2019.124509, 2020.

Dobrovolsky, I., Zubkov, S., and Miachkin, V.: Estimation of the size of earthquake preparation zones, Pure and Applied

https://doi.org/10.5194/egusphere-2025-2132
Preprint. Discussion started: 17 July 2025

624 Geophysics, 117(5), 1025-1044, 1979.

625 Du, G., Su, S., Chang, X., Ren, H., Huo, Z., and Zhang, X.: Hydrogeochemical characteristics and genesis of
626 Hongshuilantang Hot Spring and its water temperature anomalies during the Rushan earthquake swarm in Eastern
627 China, Frontiers in Earth Science, 10, https://doi.org/10.3389/feart.2022.1088240, 2023.

628 Feng, X., Zhong, J., Yan, R., Zhou, Z., Tian, L., Zhao, J., and Yuan, Z.: Groundwater Radon Precursor Anomalies
629 Identification by EMD-LSTM Model, water, 14(1), https://doi.org/10.3390/w14010069, 2022.

630 Fu, C., Yang, T., Tsai, M., Lee, L., Liu, T., Walia, V., Chen, C., Chang, W., Kumar, A., and Lai, T.: Exploring the relationship
631 between soil degassing and seismic activity by continuous radon monitoring in the Longitudinal Valley of eastern
632 Taiwan, Chemical Geology, 469, 163-175, https://doi.org/10.1016/j.chemgeo.2016.12.042, 2017.

633 Gori, F., Barberio, M. D.: Hydrogeochemical changes before and during the 2019 Benevento seismic swarm in central-
634 southern Italy, Journal of Hydrology, 604, https://doi.org/10.1016/j.jhydrol.2021.127250, 2022.

635 Haider, T., Barkat, A., Hayat, U., Ali, A., Awais, M., Alam, A., Rehman, K., and Shah, M. A.: Identification of radon
636 anomalies induced by earthquake activity using intelligent systems, Journal of Geochemical Exploration, 222,
637 https://doi.org/10.1016/j.gexplo.2020.106709, 2021.

638 Hanks, T. C., and Kanamori, H.: A moment magnitude scale. Journal of Geophysical Research: Solid Earth, 84(B5), 2348-
639 2350, https://doi.org/10.1029/JB084iB05p02348, 1979.

640 Hosono, T., and Masaki, Y.: Post-seismic hydrochemical changes in regional groundwater flow systems in response to the
641 2016 M_w7.0 Kumamoto earthquake, Journal of Hydrology, 580, https://doi.org/10.1016/j.jhydrol.2019.124340, 2020.

642 Hosono, T., Yamada, C., Manga, M., Wang, C. Y., and Tanimizu, M. Stable isotopes show that earthquakes enhance
643 permeability and release water from mountains, Nat Commun, 11(1), 2776, https://doi.org/10.1038/s41467-020-
644 16604-y, 2020.

https://doi.org/10.5194/egusphere-2025-2132
Preprint. Discussion started: 17 July 2025

645 Ide, K., Hosono, T., Kagabu, M., Fukamizu, K., Tokunaga, T., and Shimada, J.: Changes of groundwater flow systems after
646 the 2016 M_w7.0 Kumamoto earthquake deduced by stable isotopic and CFC-12 compositions of natural springs,
647 Journal of Hydrology, 583, https://doi.org/10.1016/j.jhydrol.2020.124551, 2020.
648 Ingebritsen, S. E., and Manga, M.: Hydrogeochemical precursors. Nature Geoscience, 7(10), 697-698,
649 https://doi.org/10.1038/ngeo2261, 2014.
650 Ingebritsen, S. E., and Manga, M.: Earthquake Hydrogeology. Water Resources Research, 55(7), 5212-5216,
651 https://doi.org/10.1029/2019wr025341, 2019.
652 Kim, J., Lee, J., Petitta, M., Kim, H., Kaown, D., Park, I., Lee, S., and Lee, K.: Groundwater system responses to the 2016
653 M_L5.8 Gyeongju earthquake, South Korea. Journal of Hydrology, 576, 150-163,
654 https://doi.org/10.1016/j.jhydrol.2019.06.044, 2019.
655 Lee, S., Cheong, J., Park, Y., Ha, K., Kim, Y., Kim, S., and Hamm, S.: Groundwater level changes on Jeju Island associated
656 with the Kumamoto and Gyeongju earthquakes, Geomatics, Natural Hazards and Risk, 8(2), 1783-1791,
657 https://doi.org/10.1080/19475705.2017.1387181, 2017.
658 Li, C., Zhou, X., Yan, Y., Ouyang, S., and Liu, F.: Hydrogeochemical Characteristics of Hot Springs and Their Short-Term
659 Seismic Precursor Anomalies along the Xiaojiang Fault Zone, Southeast Tibet Plateau, water, 13(19),
660 https://doi.org/10.3390/w13192638, 2021.
661 Li Y., Chen Z., Hu L., Su S., Zheng C., Liu Z., Lu C., Zhao Y., Liu J., He H., Sun F., Xu C., Zhou X., Du J., Xu S., and
662 Zheng G.: Advances in seismic fluid geochemistry and its application in earthquake forecasing (in Chinese with
663 English abstract), Chinese Science Bulletin, 67(13), 1404-1420, https://doi: 10.1360/TB-2021-0955, 2022.
664 Li Y., Fang Z., Zhang C., Li J., Bao Z., Zhang X., Liu Z., Zhou X., Chen Z., and Du J.: Research progress and prospect of
665 seismic fluid geochemistry in short-imminent earthquake prediction (in Chinese with English abstract), Seismology

https://doi.org/10.5194/egusphere-2025-2132
Preprint. Discussion started: 17 July 2025

and Geology, 45(3), 593-621, https://doi:10.3969 /j.issn.0253- 4967.2023.03.001, 2023.

Li, Y., Gao, Y., Tian, J., and Wang, Q.: Rayleigh phase velocity and azimuthal anisotropy from high dense seismic arrays reveal strong control of block boundary faults on crustal material migration in SW China, Journal of Asian Earth Sciences, 276, https://doi.org/10.1016/j.jseaes.2024.106337, 2024.

Li, Y., Liu, M., Li, Y., and Chen, L.: Active crustal deformation in southeastern Tibetan Plateau: The kinematics and dynamics, Earth and Planetary Science Letters, 523, https://doi.org/10.1016/j.epsl.2019.07.010, 2019.

Martinelli, G.: Previous, Current, and Future Trends in Research into Earthquake Precursors in Geofluids, Geosciences, 10(5), https://doi.org/10.3390/geosciences10050189, 2020.

Ma, L., Qiao, X., Min, L., Fan, B., and Ding, X.: Geological Atlas of China (in Chinese), Geology Press, Beijing, pp. 1-348, 2002.

Nakagawa, K., Yu, Z., Berndtsson, R., and Hosono, T.: Temporal characteristics of groundwater chemistry affected by the 2016 Kumamoto earthquake using self-organizing maps. Journal of Hydrology, 582, https://doi.org/10.1016/j.jhydrol.2019.124519, 2020.

Petitta, M., Mastrorillo, L., Preziosi, E., Banzato, F., Barberio, M. D., Billi, A., Cambi, C., De Luca, G., Di Carlo, G., Di Curzio, D., Di Salvo, C., Nanni, T., Palpacelli, S., Rusi, S., Saroli, M., Tallini, M., Tazioli, A., Valigi, D., Vivalda, P., and Doglioni, C.: Water-table and discharge changes associated with the 2016-2017 seismic sequence in central Italy: hydrogeological data and a conceptual model for fractured carbonate aquifers, Hydrogeology Journal, 26(4), 1009-1026, https://doi.org/10.1007/s10040-017-1717-7, 2018.

Piersanti, A., Cannelli, V., and Galli, G.: The Pollino 2012 seismic sequence: clues from continuous radon monitoring. Solid Earth, 7(5), 1303-1316, https://doi.org/10.5194/se-7-1303-2016, 2016.

Pritchard, M. E., Allen, R. M., Becker, T. W., Behn, M. D., Brodsky, E. E., Bürgmann, R., Ebinger, C., Freymueller, J. T.,

https://doi.org/10.5194/egusphere-2025-2132
Preprint. Discussion started: 17 July 2025

687 Gerstenberger, M., Haines, B., Kaneko, Y., Jacobsen, S. D., Lindsey, N., McGuire, J. J., Page, M., Ruiz, S., Tolstoy,
688 M., Wallace, L., Walter, W. R., Wilcock, W., and Vincent, H.: New Opportunities to Study Earthquake Precursors,
689 Seismological Research Letters, 91(5), 2444-2447, https://doi.org/10.1785/0220200089, 2020.
690 Ruggieri, E.: A Bayesian approach to detecting change points in climatic records, International Journal of Climatology,
691 33(2), 520-528, https://doi.org/10.1002/joc.3447, 2012.
692 Schoenbohm, L. M., Burchfiel, B. C., Liangzhong, C., and Jiyun, Y.: Miocene to present activity along the Red River fault,
693 China, in the context of continental extrusion, upper-crustal rotation, and lower-crustal flow, Geological Society of
694 America Bulletin, 118(5-6), 672-688, https://doi.org/10.1130/b25816.1, 2006.
695 Shao, W., Liu, Z., Li, Y., Chen, Z., Lu, C., Zhao, C., Wang, Y., Li, Q., Gao, Z., Luo, Y., Ran, H., and Fan, S.: Geochemical
696 Characteristics of Thermal Springs and Insights Into the Intersection Between the Xiaojiang Fault and the Red River
697 Fault, Southeastern Tibet Plateau, Geochemistry, Geophysics, Geosystems, 25(3),
698 https://doi.org/10.1029/2023gc011431, 2024.
699 Shi, Z., Wang, G., Manga, M., and Wang, C.: Mechanism of co-seismic water level change following four great
700 earthquakes-insights from co-seismic responses throughout the Chinese mainland, Earth and Planetary Science Letters,
701 430, 66-74, https://doi.org/10.1016/j.epsl.2015.08.012, 2015.
702 Shi, Z., Zhang, H., and Wang, G.: Groundwater trace elements change induced by M5.0 earthquake in Yunnan, Journal of
703 Hydrology, 581, https://doi.org/10.1016/j.jhydrol.2019.124424, 2020.
704 Skelton, A., Andrén, M., Kristmannsdóttir, H., Stockmann, G., Mörth, C. M., Sveinbjörnsdóttir, Á., Jónsson, S., Sturkell,
705 E., Guðrúnardóttir, H. R., Hjartarson, H., Siegmund, H., and Kockum, I.: Changes in groundwater chemistry before
706 two consecutive earthquakes in Iceland, Nature Geoscience, 7(10), 752-756, https://doi.org/10.1038/ngeo2250, 2014.
707 Soldati, G., Cannelli, V., and Piersanti, A.: Monitoring soil radon during the 2016-2017 central Italy sequence in light of

https://doi.org/10.5194/egusphere-2025-2132
Preprint. Discussion started: 17 July 2025

seismicity. Sci Rep, 10(1), 13137, https://doi.org/10.1038/s41598-020-69821-2, 2020.

Tapponnier, P., Peltzer, G., Le Dain, A. Y., Armijo, R., and Cobbold, P.: Propagating extrusion tectonics in Asia: New insights from simple experiments with plasticine, Geology, 10(12), https://doi.org/10.1130/0091-7613(1982)10, 1982.

Tareen, A. D. K., Asim, K. M., Kearfott, K. J., Rafique, M., Nadeem, M. S. A., Iqbal, T., and Rahman, S. U.: Automated anomalous behaviour detection in soil radon gas prior to earthquakes using computational intelligence techniques, J Environ Radioact, 203, 48-54, https://doi.org/10.1016/j.jenvrad.2019.03.003, 2019.

Taylor, R. G., Todd, M. C., Kongola, L., Maurice, L., Nahozya, E., Sanga, H., and MacDonald, A. M.: Evidence of the dependence of groundwater resources on extreme rainfall in East Africa, Nature Climate Change, 3(4), 374-378, https://doi.org/10.1038/nclimate1731, 2012.

Thomas, D.: Geochemical precursors to seismic activity, Pure and Applied Geophysics, 126, 241-266, 1988.

Tian, J., Zhou, X., Yan, Y., He, M., Li, J., Dong, J., Liu, F., Ouyang, S., Li, Y., Tian, L., Wang, Y., Huang, T., and Pang, Z.: Earthquake-induced impulsive release of water in the fractured aquifer system: Insights from the long-term hydrochemical monitoring of hot springs in the Southeast Tibetan Plateau, Applied Geochemistry, 148, https://doi.org/10.1016/j.apgeochem.2022.105553, 2023.

Tian J., Zhu R., Ju C., Tian L., and Zhou X.: Research progress on chemical change of hot spring water in earthquake monitoring and prediction (in Chinese with English abstract), Earthquake, 44(4), 97-115, https://doi:10.12196/j.issn.1000-3274.2024.04.007, 2024.

Tong, Y., Yang, Z., Wang, H., Gao, L., An, C., Zhang, X., and Xu, Y.: The Cenozoic rotational extrusion of the Chuan Dian Fragment: New paleomagnetic results from Paleogene red-beds on the southeastern edge of the Tibetan Plateau, Tectonophysics, 658, 46-60, https://doi.org/10.1016/j.tecto.2015.07.007, 2015.

Wang, B., Zhou, X., Zhou, Y., Yan, Y., Li, Y., Ouyang, S., Liu, F., and Zhong, J.: Hydrogeochemistry and Precursory

https://doi.org/10.5194/egusphere-2025-2132
Preprint. Discussion started: 17 July 2025

729 Anomalies in Thermal Springs of Fujian (Southeastern China) Associated with Earthquakes in the Taiwan Strait, water,
730 13(24), https://doi.org/10.3390/w13243523, 2021.
731 Wang, C. Y., and Manga, M.: Hydrologic responses to earthquakes and a general metric, Geofluids, 10(1-2), 206-216,
732 https://doi.org/10.1111/j.1468-8123.2009.00270.x, 2010.
733 Wang, Y., Zhang, B., Hou, J., and Xu, X.: Structure and tectonic geomorphology of the Qujiang fault at the intersection of
734 the Ailao Shan–Red River fault and the Xianshuihe–Xiaojiang fault system, China, Tectonophysics, 634, 156-170,
735 https://doi.org/10.1016/j.tecto.2014.07.031, 2014.
736 Wen, X., Ma, S., Xu, X., and He, Y.: Historical pattern and behavior of earthquake ruptures along the eastern boundary of
737 the Sichuan-Yunnan faulted-block, southwestern China, Physics of the Earth and Planetary Interiors, 168(1-2), 16-36,
738 https://doi.org/10.1016/j.pepi.2008.04.013, 2008.
739 Wen, X., Du, F., Long, F., Fan, J., and Zhu, H.: Tectonic dynamics and correlation of major earthquake sequences of the
740 Xiaojiang and Qujiang-Shiping fault systems, Yunnan, China, Science China Earth Sciences, 54(10), 1563-1575,
741 https://doi.org/10.1007/s11430-011-4231-0, 2011.
742 Wen, X., Ma, S., Fang, L., Liang, M., Du, F., Long, F., and Zhao, X.: Complex structural fault system and distributed
743 deformation across the Big Bend of the Red River fault, Yunnan, China, Physics of the Earth and Planetary Interiors,
744 333. https://doi.org/10.1016/j.pepi.2022.106942, 2022.
745 Woith, H.: Radon earthquake precursor: A short review, The European Physical Journal Special Topics, 224(4), 611-627,
746 https://doi.org/10.1140/epjst/e2015-02395-9, 2015.
747 Woith, H., Daskalopoulou, K., Zimmer, M., Fischer, T., Vlček, J., Trubač, J., Rosberg, J. E., Vylita, T., and Dahm, T.: Multi-
748 Level Gas Monitoring: A New Approach in Earthquake Research, Frontiers in Earth Science, 8,
749 https://doi.org/10.3389/feart.2020.585733, 2020.

https://doi.org/10.5194/egusphere-2025-2132
Preprint. Discussion started: 17 July 2025

Xu Z., Li H., Tang Z., Qi X., Li H., and Cai Z.: The transformation of the terrain structures of the Tibet Plateau through large-scale strike-slip faults (in Chinese with English abstract), Acta Petrologica Sinica, 27(11), 3157-3170, 2011.

Yan R., Tian L., Wang G., Zhong J., Liu J., and Zhou Z.: Review and statistically characteristic analysis of underground fluid anomalies prior to the 2008Wenchuan M_S8.0 earthquake (in Chinese with English abstract), Chinese J. Geophys, 61(5), 1907-1921, https://doi:10.6038/cjg2018M0162, 2018.

Yan, X., Shi, Z., Wang, G., Zhang, H., and Bi, E.: Detection of possible hydrological precursor anomalies using long short-term memory: A case study of the 1996 Lijiang earthquake, Journal of Hydrology, 599, https://doi.org/10.1016/j.jhydrol.2021.126369, 2021.

Yan, Y., Zhou, X., Liao, L., Tian, J., Li, Y., Shi, Z., Liu, F., and Ouyang, S.: Hydrogeochemical Characteristic of Geothermal Water and Precursory Anomalies along the Xianshuihe Fault Zone, Southwestern China, water, 14(4), https://doi.org/10.3390/w14040550, 2022.

Yin, A., and Harrison, T. M.: Geologic evolution of the Himalayan-Tibetan orogen, Annual Review of Earth and Planetary Sciences, 28, 211-280, https://doi.org/10.1146/annurev.earth.28.1.211, 2000.

Zhang, L., Guo, L., Zhou, X., Yang, Y., Shi, D., and Liu, Y.: Temporal variations in stable isotopes and synchronous earthquake-related changes in hot springs, Journal of Hydrology, 599, https://doi.org/10.1016/j.jhydrol.2021.126316, 2021.

Zhang P., Deng Q., Zhang G., Ma J., Gan W., Min W., Mao F., and Wang Q.: The strong earthquake activities and active tectonic blocks in China mainland (in Chinese), Science China Series D: Earth Sciences, 33(S1): 12-20, 2003.

Zhang, W., Li, M., Yang, Y., Rui, X., Lu, M., and Lan, S.: Implications of groundwater level changes before near field earthquakes and its influencing factors - several earthquakes in the vicinity of the Longmenshan-Anninghe fault as an example, Frontiers in Earth Science, 13. https://doi.org/10.3389/feart.2025.1541346, 2025.

https://doi.org/10.5194/egusphere-2025-2132
Preprint. Discussion started: 17 July 2025

771 Zhao, Y., Liu, Z., Li, Y., Hu, L., Chen, Z., Sun, F., and Lu, C.: A case study of 10 years groundwater radon monitoring
772 along the eastern margin of the Tibetan Plateau and in its adjacent regions: Implications for earthquake surveillance,
773 Applied Geochemistry, 131, https://doi.org/10.1016/j.apgeochem.2021.105014, 2021.
774 Zhou, X., Yan, Y., Fang, W., Wang, W., Shi, H., and Li, P.: Short-Term Seismic Precursor Anomalies of Hydrogen
775 Concentration in Luojishan Hot Spring Bubbling Gas, Eastern Tibetan Plateau, Frontiers in Earth Science, 8,
776 https://doi.org/10.3389/feart.2020.586279, 2021.
777 Zhu, R., Yang, F., Zhou, X., Tian, J., Zhang, Y., He, M., Li, J., Dong, J., and Li, Y.: Anomaly Detection Using Machine
778 Learning in Hydrochemical Data From Hot Springs: Implications for Earthquake Prediction, Water Resources
779 Research, 60(6), https://doi.org/10.1029/2023wr034748, 2024.
780